

A correlation-based analysis on wind-induced interference effects between two tall buildings

Z. N. Xie[†] and M. Gu[‡]

*State Key Laboratory for Disaster Reduction in Civil Engineering, Tongji University,
Shanghai 200092, People's Republic of China*

(Received August 13, 2003, Accepted January 21, 2005)

Abstract. Wind-induced mean and dynamic interference effects of tall buildings are studied in detail by a series of wind tunnel tests in this paper. Interference excitations of several types of upwind structures of different sizes in different upwind terrains are considered. Comprehensive interference characteristics are investigated by artificial neural networks and correlation analysis. Mechanism of the wakes vortex-induced resonance is discussed, too. Measured results show significant correlations exist in the distributions of the interference factors of different configurations and upwind terrains and, therefore, a series of relevant regression equations are proposed to simplify the complexity of the multi-parameter wind induced interference effects between two tall buildings.

Keywords: tall building; interference effects; wind load; correlation method; regression analysis.

1. Introduction

Wind loads on buildings in realistic environments may be quite different from those measured on isolated buildings. Surrounding or upstream buildings can significantly increase or decrease the flow-induced forces on a building, depending mainly on the arrangement and geometry of these buildings, wind velocity and direction, type of upstream terrain etc., Bailey and Kwok (1985) investigated the enhanced dynamic response of a tall square building under the interference action from the neighbouring square and circular buildings. Two-dimensional contour maps were used in their study to describe the variation of the interference factor (*IF*) with the position of the interfering building. With these contours, the critical location for the interfering building and the extent of the interference effect can be easily found. Taniike and Inaoka (1988) and Taniike (1991) investigated the increased response and the possible aeroelastic mechanism of a tall square building under the interference excitation of several types of upstream buildings with different breadths in different upstream flow conditions. The effects of different parameters on the interference effects of tall buildings have been investigated by many other researchers in the past thirty years or so. Khanduri, *et al.* (1998) gave a detailed review of the state-of-the-art on the investigations of the wind-induced interference effects on buildings.

[†] Professor, currently, Dept. of Civil Engineering, Shantou University, Shantou 515063

[‡] Professor, Corresponding Author, Tel. and Fax: +86-21-65981210, E-mail: minggu@mail.tongji.edu.cn

However, it is not easy to get a fully understanding or obtain the empirical generalizations of the interference effects on tall buildings. The difficulty results from the complexity of the problem, a large number of parameters affecting the interference effect, the scarcity of adequate experimental data, and the inconsistencies among the results of various studies. Researchers are still devoted to tackle the problem in a systematic manner in order to propose a generalized set of guidelines that will be useful for building designers and planners. English (1993) suggested a third-order regression polynomial to predict shielding factors for a pair of rectangular prisms in tandem. Khanduri, *et al.* (1997) and English and Fricke (1999) applied the artificial neural networks (ANN) method to predict the wind induced interference effects by training the ANN with the existed incomplete or even confusing experimental data.

This paper aims at providing a quantitative analysis to determine the effects of different variables on the mean and dynamic interference effects between two square tall buildings. The interference effects between two identical tall buildings and the effects of the breadth and height of the interfering building and the upstream terrain conditions are quantitatively analyzed by using of correlation analysis and the ANN-based method. Some primary suggestions are proposed for the assessment of wind-induced interference effects on design loads for tall buildings.

2. Description of experiment and analysis

2.1. Experimental equipment

The wind tunnel tests are conducted in the STDX-1 Boundary Wind Tunnel of the Department of Civil Engineering at Shantou University. The main test section of STDX-1 for the building model is 20 m long, 3 m wide and 2 m high. The test section has an adjustable roof that provides a negligible pressure gradient in the downstream direction. The maximum wind speed of the wind tunnel can reach 45 m/s. According to the Chinese Load Code (GB50009-2001), the exposure categories B and D (corresponding to exponents of the power law of mean speed profile of 0.16 and 0.30, respectively) are simulated by setting spires, barriers, and rough elements in the test area. The simulated mean wind profiles (V/V_g) and turbulence intensity distributions $\varepsilon(\%)$ for the two exposure categories are shown in Fig. 1, where V_g is the mean wind speed at the gradient wind height.

The measurements in this paper are carried out by means of the Nitta's universal force-moment sensor model No. UFS-4515A100 and the attached signal conditioner and amplifier. The technical specifications for the sensor are shown in Table 1.

The conditioned and amplified analog signal from the sensor is filtered by the low pass filters in the system, transmitted to a Scanivalve's Zoc/EIM-16 module, and eventually converted quickly by the Scanivalve's sampling platform. The natural frequencies of the sensor are very high and the fundamental frequency of the sensor and lightweight-rigid-model system can reach up to 112 Hz. Moreover, an additional treatment is made to revise the distorted signal in the high frequency band that could improve the measurement accuracy on the power spectrum density (PSD) of the overturning moments.

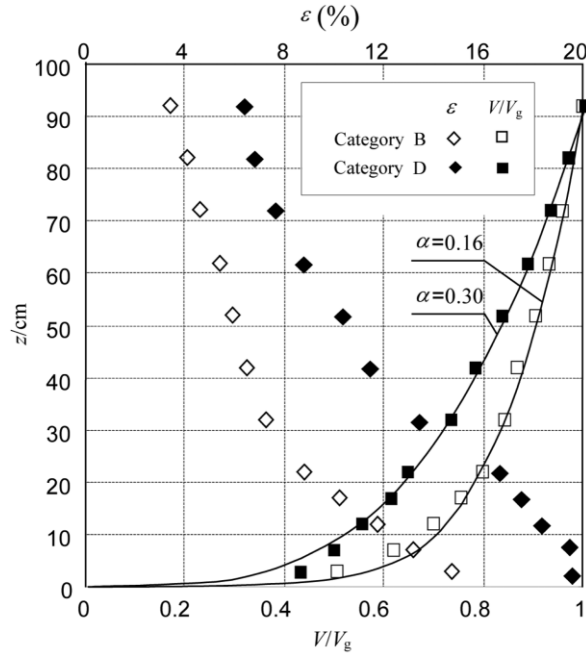


Fig. 1 Wind profiles and turbulence intensity distributions

Table 1 Specifications of Nitta UFS-4515A100 sensor

Component	Full scale range	Accuracy
$F_x \cdot F_y$	440N	
F_z	880N	Linearity: 0.2%F.S. Hysteresis: 0.2%F.S.
$M_x \cdot M_y \cdot M_z$	51N·m	

2.2. Experimental arrangements

A 600 mm tall and 100 mm wide square model, made of light foam and skinned with lightweight wood, is used as the principal building. The corresponding dynamic characteristics of the prototype are: height of 240 m; breadth of 40 m; structural damping of $\zeta = 2\%$ of critical damping; and natural frequency of $f_0 = 0.2$ Hz for both sway fundamental modes. Other two groups of upstream building models are used as the interfering buildings. The first group of interfering buildings has the same height (600 mm) as the principal building, and square cross sections with different breadths of $0.5b$, $0.75b$, $1b$, $1.5b$ and $2.0b$, where b (= 100 mm) is the breadth of the principal building model. The second group of interfering buildings has the same cross section as the principal building but with different heights of $0.5h$, $0.75h$, $1h$, $1.25h$ and $1.5h$, where h is the height of the principal building model. All the building models are orientated with one face normal to the wind direction and the spacing between them varies as the test parameters in the along-wind direction (x) and the across-wind direction (y) in a grid system as shown in Fig. 2, where A is the interfering building, and C the principal building at (0,0).

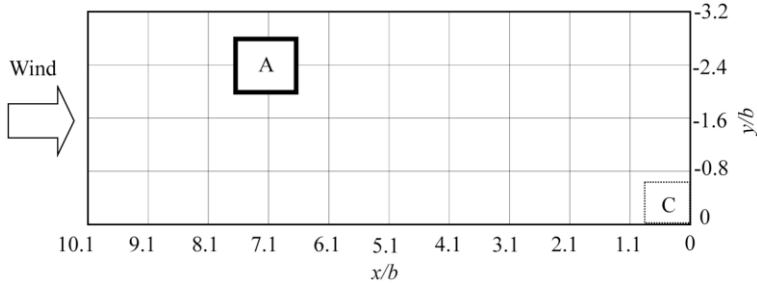


Fig. 2 x - y coordinate grid for locating the interfering building, principal building is fixed at (0, 0)

2.3. Formulation

According to the theory of high frequency base force balance (Tschanz and Davenport 1983), the power spectral density (PSD) and the rms value of the dynamic response base moment, $S_{M_D}(f)$ and σ_{M_D} , may be written as

$$S_{M_D}(f) = |H(f)|^2 S_{M_s}(f) \quad (1)$$

$$\sigma_{M_D} = \sqrt{\int_0^\infty |H(f)|^2 S_{M_s}(f) df} \approx \sigma_{M_s} \sqrt{1 + \frac{\pi}{4} \frac{1}{\zeta_0} \frac{\chi_0 S_{M_s}(\chi_0)}{\sigma_{M_s}^2}} \quad (2)$$

in which

$$|H(f)|^2 = \frac{1}{\left(1 - \left(\frac{f}{f_0}\right)^2\right)^2 + \left(2\zeta_0 \frac{f}{f_0}\right)^2} \quad (3)$$

is the mechanical admittance, $\{\chi S_{M_s}(\chi) / \sigma_{M_s}^2\}$ denotes the dimensionless PSD of the base moment, $M_s(t)$ can be directly measured by the high frequency base force balance. σ_{M_s} is the rms value of $M_s(t)$. $\chi_0 = f_0 D / V_H$ is the reduced natural frequency, D is the characteristic breadth of the structure, and V_H is the mean velocity at the top of the structure. The reciprocal of the reduced frequency χ_0 is the reduced velocity, i.e.,

$$V_r = \frac{1}{\chi_0} = \frac{V_H}{f_0 D} \quad (4)$$

So one can find that the dynamic response base moment varies with the reduced velocity. Considering the effects of the nearby buildings, the so-called interference effects on the principal building are commonly expressed in term of an interference factor (*IF*) given by

$$IF = \frac{\text{Wind load on a building with interference buildings present}}{\text{Wind load on an isolated building}} \quad (5)$$

where the wind load can be the mean along-wind base moment or the rms value of the dynamic response base moments in the along-wind or the across-wind direction. It can be seen that the dynamic *IFs* vary with the reduced velocity, too. In order to simplify the complexity of the problem,

the envelope value of the dynamic interference factor (*EIF*) is applied to describe the dynamic interference effects by maximizing the *IFs* in the reduced velocity ranges of $V_r = 2 \sim 9$, i.e.,

$$EIF = \max_{V_r \in [2, 9]} IF(V_r) \quad (6)$$

where the higher reduced velocities of $V_r > 9$ rarely happen for the practical structures and are not considered. Of course, the mean interference factors are independent of the reduced velocity.

Data analysis on the interference effects conducted in this study is a complex task. A Windows-based software platform that integrates spectrum computation, artificial neural network, and correlation analysis is thus developed to process the test data. The software system can be used to analyze the interference characteristics and mechanism and model the interference effects. With the help of this software the interference factors at other positions could be predicated by modeling the data and the interference factor contours could be drawn quickly.

3. Experimental results and discussion

3.1. Results of two identical buildings in exposure category B

Fig. 3 shows the interference factor distributions of the mean along-wind base moment and the rms value of the dynamic response base moments on the principal building due to the interference effects caused by the identical interfering building at various upstream locations in exposure category B.

The variation of mean along-wind moments with spacing between two buildings is indicated in Fig. 3(a). It can be seen that the effects of the upstream interfering building show generally shielding effects, i.e., $IF < 1$. Clearly the maximum shielding occurs when two buildings are in tandem position, and the closer the interfering building, the more significant the shielding effects. It can be found that the contour has a negative zone corresponding to the negative *IF*, which indicates that the principal building is subjected to a converse wind drag force. In addition, a zero interference factor is found at about $x/b = 3$ in tandem arrangement. This position is almost consistent with the result observed by Sakamoto and Haniu (1988) in a similar terrain condition of open terrain.

The variation of dynamic wind loads due to the interference action follows a different trend from those of the mean wind loads. The results show that the effects are much more severe since the recorded *EIFs* are much more greater than the *IF* of the mean wind load, and the *EIFs* greater than 1 are measured at most locations. Fig. 3(b) shows the distributions of the along-wind envelope dynamic interference factors. An *EIF* as high as 2.42 is measured at $x/b = 4.1$, $y/b = -0.8$. The significant along-wind interference effects are found when the principal building is located near the high-speed wake boundary of the upstream interfering building. The increased turbulence and mean velocity induced by the upstream building are the key reasons that affect the along-wind dynamic response of the principal building.

Fig. 3(c) shows the distributions of the across-wind envelope dynamic interference factors. The significant interference location of the interfering building is found in the region ($x/b = 3 \sim 10$, $y/b = 1.8 \sim 3.2$) at which the *EIFs* greater than 2 are recorded and the maximum *EIF* in this region is found up to 2.42 (the same as the along-wind dynamic interference effects) at $x/b = 9.1$, $y/b = 3.2$. However, different from the along-wind response, the most significant across-wind interference effect of the interfering building is found at the critical location of $x/b = 0$, $y/b = -2.4$ (i.e. the two buildings are arranged side-by-side and with a spacing of $2.4b$) which produces an *EIF* of 2.53.

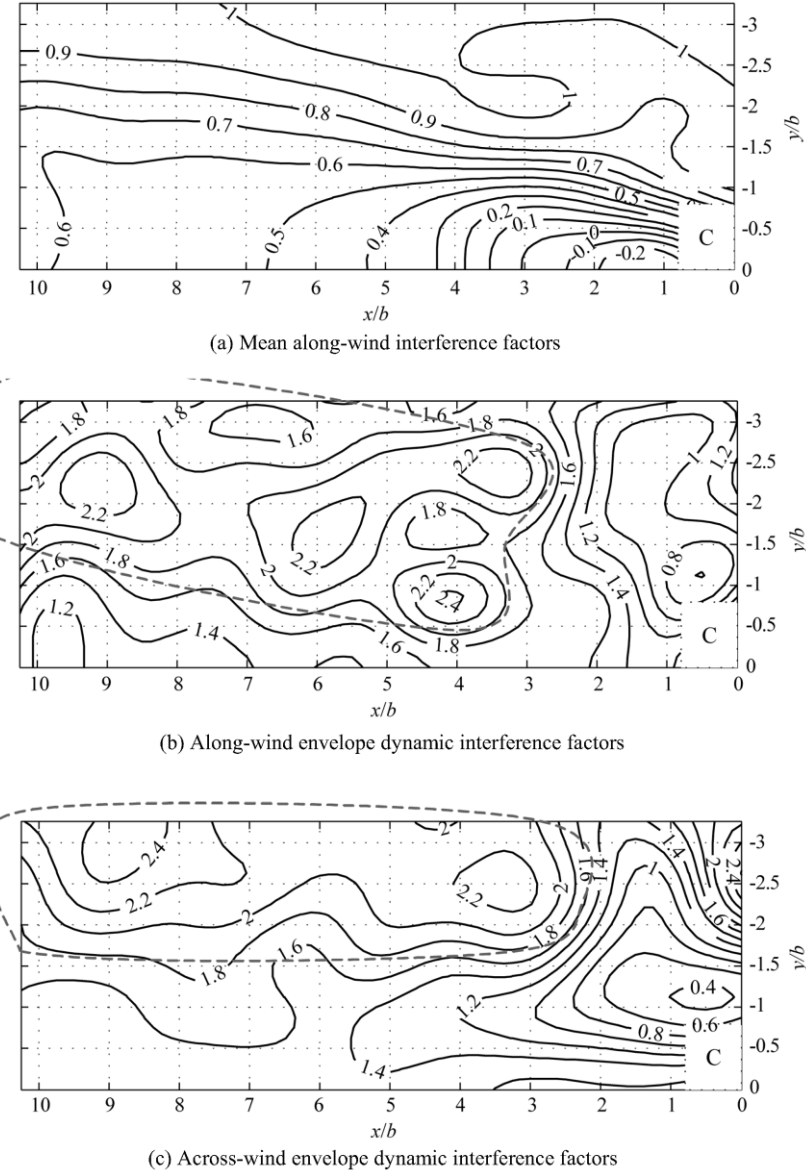


Fig. 3 Contours of the interference factors of two identical buildings (in exposure category B)

Another *EIF* of 2.2 is found when the interfering building at $x/b = 0$, $y/b = -3.2$. This indicates that the side-by-side arranged interfering building can significantly affects the across-wind loads on the principal building.

3.2. Effects of size of the interfering buildings

To investigate the effects of the breadth ratio (hereafter referred to as B_r) of the across-section of the interfering buildings to the principal building and the height ratio (hereafter referred to as H_r) of

the interfering buildings to the principal building on the interference factors, two groups of upstream interfering building models are adopted. The first group of interfering buildings has the same height as the principal building but with different B_r of 0.5, 0.75, 1, 1.5 and 2.0. The second group of interfering buildings has the same cross-section as the principal building but with different H_r of 0.5, 0.75, 1, 1.25 and 1.5. The results from the test in exposure category B are discussed in the following.

3.2.1. Effect of breadth ratio

3.2.1.1. Mean interference effect

Generally, larger B_r of interfering building produces stronger shielding effects. In most of the interfering positions, the interference factor decreases with the increase of B_r . In order to quantify the effect of B_r , the $IF(x/b, y/b)$ of the four configurations of $B_r=0.5, 0.75, 1.5$ and 2 are compared with the $IF(x/b, y/b)$ of the configuration of $B_r=1$. The results are shown in Fig. 4.

In Fig. 4, the data are regressed as linear expression since the stronger correlations can be seen

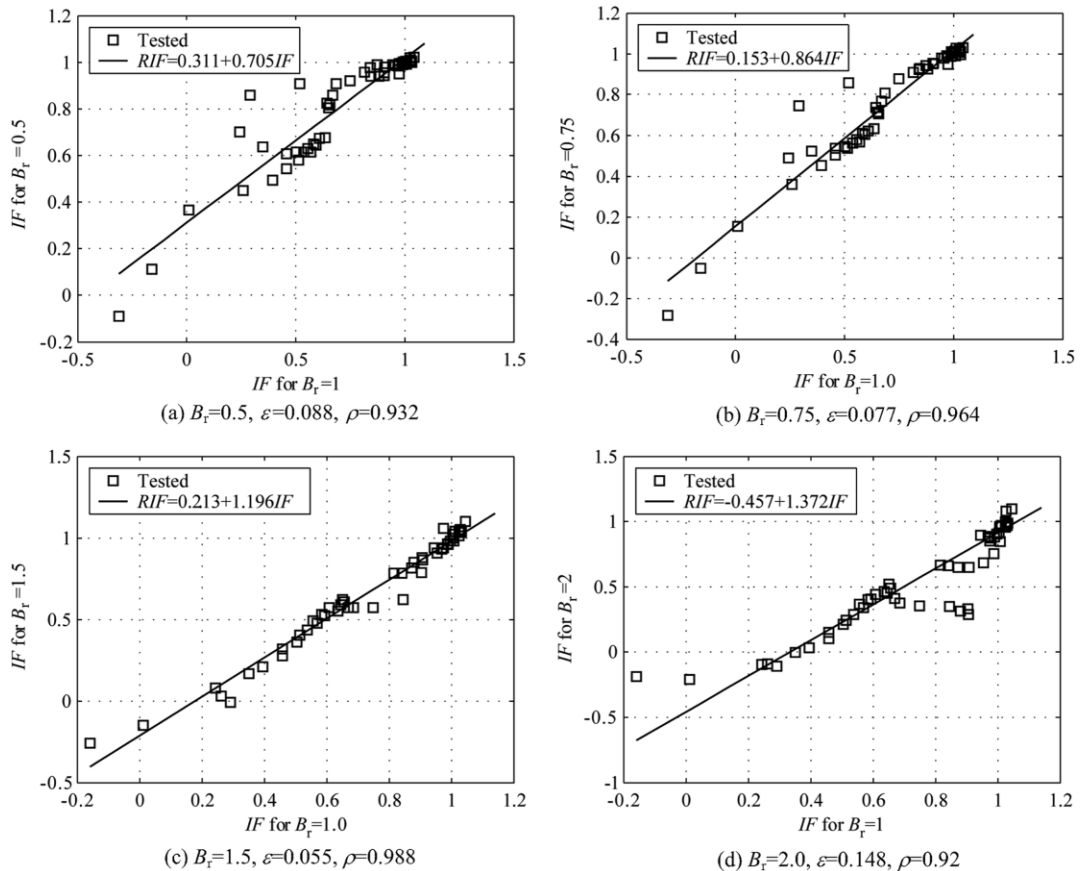


Fig. 4 Correlation analysis of the mean interference factors for the configurations of different breadth ratios

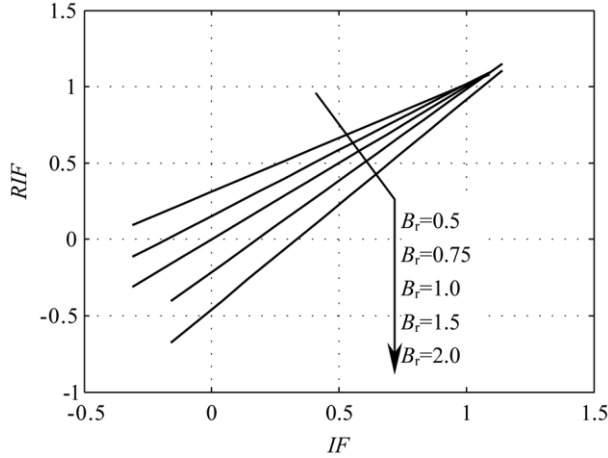


Fig. 5 Comparison of the regression results of the mean *IF* for the configurations of different breadth ratios

between the two sets of the test *IFs*; *RIF* is the linear regression interference factor; ε is residual, denoting the accuracy of the regression and ranging from 0.05 to 0.148; ρ is the correlation coefficient that denotes the degree of the correlations and is found in the range of 0.92 to 0.99. The closer the value of the correlation coefficient is to 1, the better linear correlation between the two sets of the test *IFs* data. The regression relations of the *IFs* for different configuration of B_r , can be summarized as

$$RIF = \begin{cases} 0.311 + 0.705IF & B_r = 0.5 \\ 0.153 + 0.864IF & B_r = 0.75 \\ IF & B_r = 1.0 \\ -0.213 + 1.196IF & B_r = 1.5 \\ -0.457 + 1.372IF & B_r = 2.0 \end{cases} \quad (7)$$

From Eq. (7) one can predict the *IF* of $B_r \neq 1$ from the distribution of the *IF* of two identical buildings as shown in Fig. 3(a). The variations of the *RIF* with various B_r of the interfering building are presented in Fig. 5, which shows that the *RIF* decreases with the increase of B_r , i.e., the shielding is enhanced with the increase of the breadth of the upstream building.

3.2.1.2. Dynamic interference effect

Fig. 6 presents the distributions of the along-wind and across-wind envelope dynamic interference factors of the configurations of $B_r = 0.5, 0.75, 1.5$ and 2.0 , while the corresponding distributions of the *EIfs* for the configuration of $B_r = 1$ are shown in Fig. 3(b) and Fig. 3(c). The figures show obvious differences among the distributions of the *EIfs* for the different configurations of breadth ratios. This is mainly due to that the dynamic interference effects are sensitive to the breadth of the upstream interfering building.

It can be seen from Fig. 3(b), Fig. 3(c) and Fig. 6 that the breadth of the upstream interfering

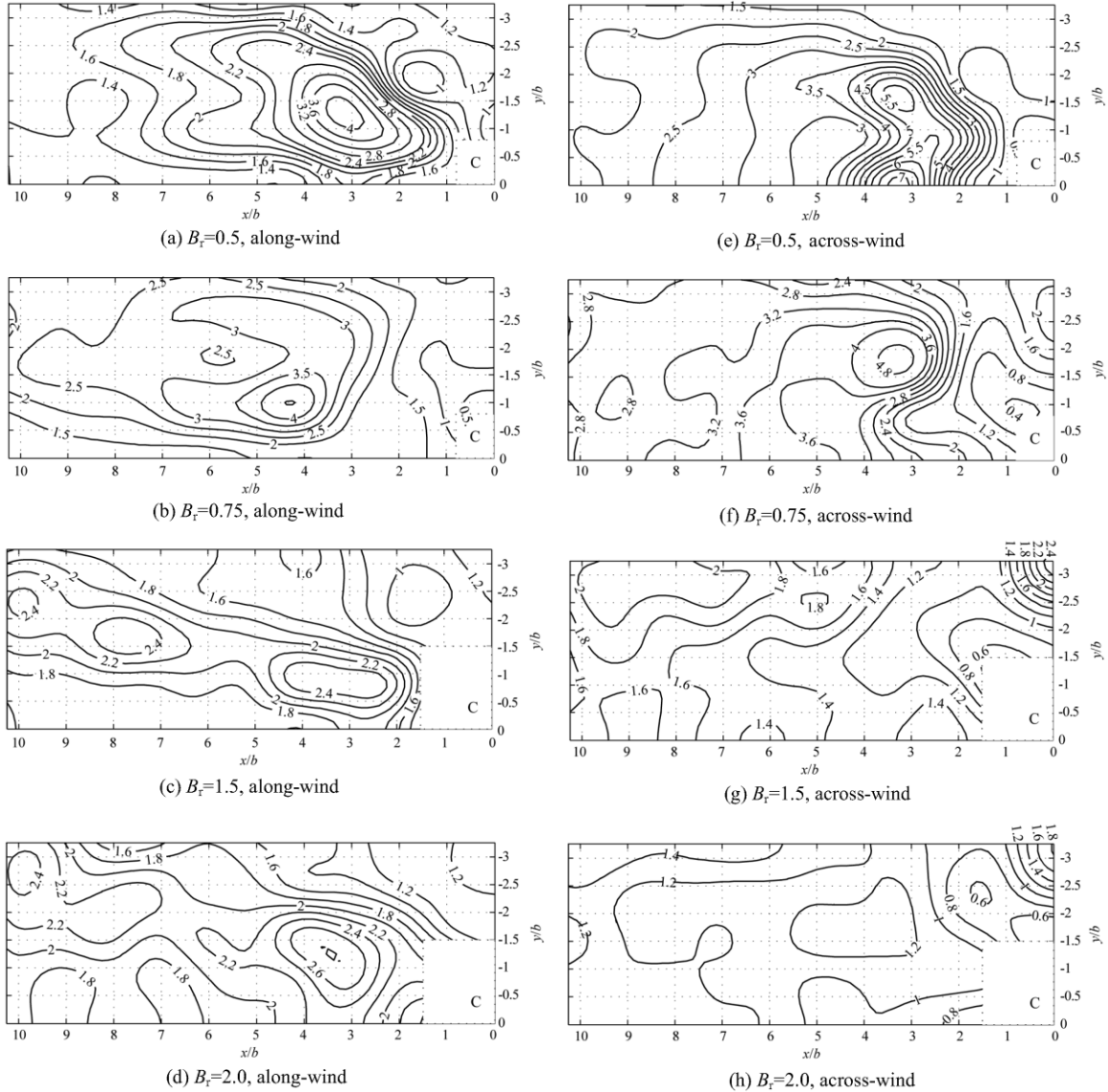


Fig. 6 Envelope dynamic interference factors for different breadth ratios ($V_r = 2\sim 9$, exposure category B)

building can significantly affect the dynamic wind loads on the down stream principal building. And the EIF distributions of two configurations of $B_r = 0.5$ and 0.75 are more pronounced than those of the other three configurations of $B_r \geq 1$. The maximum EIFs in the along-wind direction and the across-wind direction for each configuration are listed in Table 2, which shows that the maximum EIFs of the smaller breadth ratios of $B_r < 1$ are much greater than those of the larger breadth ratios of $B_r \geq 1$. This phenomenon is due to the vortex-induced resonance and will be further discussed in the following section.

Table 2 Maximum EIF of different breadth ratio configurations

B_r	Along-wind		Across-wind	
	EIF_{\max}	Critical location	EIF_{\max}	Critical location
0.5	3.81	(3.1b, -1.6b)	7.09	(3.1b, 0)
0.75	4.22	(4.1b, -0.8b)	4.83	(3.1b, -1.6b)
1.0	2.43	(4.1b, -0.8b)	2.53	(0, -2.4b)
1.5	2.53	(8.1b, -1.6b)	2.55	(0, -3.2b)
2.0	2.71	(3.1b, -0.8b)	1.82	(0, -3.2b)

3.2.1.3. Mechanism of wake vortex-induced resonance

The above-discussed larger dynamic interference factors are due to the vortex-induced resonance. This is the case when the vortex shedding frequency of the upstream structure coincides with the natural frequency of the downstream principal building. This phenomenon, defined as “resonant buffeting” in other literatures (Bailey and Kwok 1985, Taniike 1992, Zhang, *et al.* 1994), could occur at a lower reduced velocity and induce larger response of the principal building. The ratio of the vortex shedding frequency from the upstream structure to the natural frequency of the downstream building with the same height is

$$\frac{f}{f_s} = \frac{S_t V_r}{B_r} \quad (8)$$

where f is the vortex shedding frequency, f_s is the natural frequency of the principal building, and S_t is the Strouhal number of the upstream building. When the ratio of the two frequencies is equal to 1, that is when the vortex shedding frequency of the upstream structure coincides with the natural frequency of the principal downstream building, the resonance occurs. The Strouhal number of the square section buildings discussed above is about 0.1 in exposure category B and this results in the critical reduced velocity for the downstream building as

$$V_r = B_r / S_t = B_r / 0.1 = 10B_r \quad (9)$$

For the five types of interfering building with $B_r = 0.5, 0.75, 1.0, 1.5$ and 2 , the corresponding critical reduced velocities are $5, 7.5, 10, 15$ and 20 respectively. This also gives the explanation that the EIF distributions of the cases of $B_r = 0.5$ and 0.75 are more pronounced than those of the other cases as shown in Fig. 6.

Fig. 7 shows the comparison of the along-wind and the across-wind overturning moment PSD of the principal building with and without the presence of the interfering building of $B_r = 0.5$ at the corresponding critical location as shown in Fig. 6(a) and Fig. 6(e). The normalized PSD is presented as the function of the reduced frequency, fD/V_H , that is the reciprocal of the reduced velocity, $V_r = V_H/fD$. For the reduced velocity of 5 mentioned above, the corresponding reduced frequency is $fD/V_H = 1/5 = 0.2$. The variations of the IF with the reduced velocity of the above-mentioned arrangements are shown in Fig. 8.

From Figs. 7 and 8 it can be seen that the PSD of the principal building is significantly altered by the interfering building. The values of the PSD at high frequency band are enhanced and the

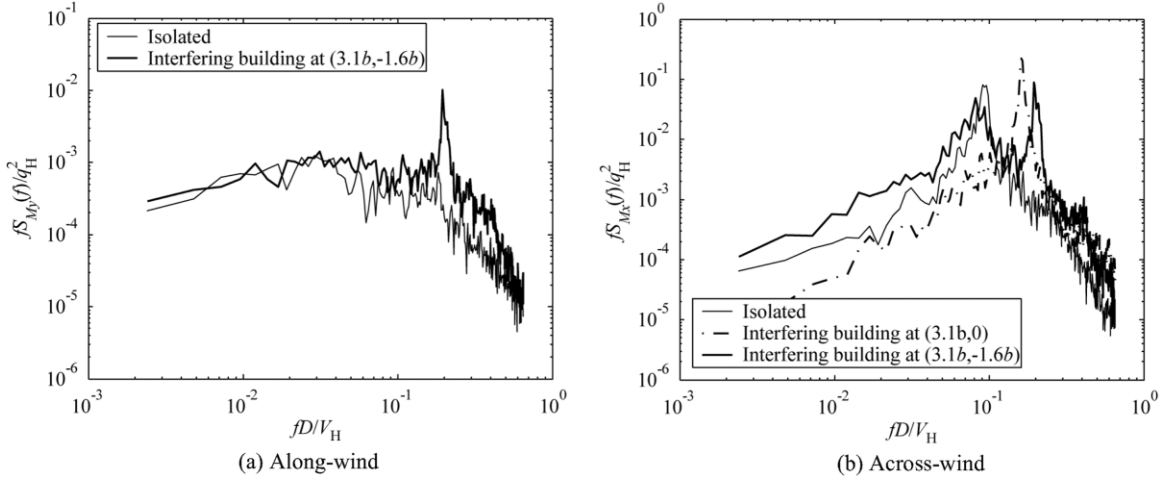


Fig. 7 Comparison of the normalized overturning moment PSD of the principal building with and without the presence of the interfering building of $B_r=0.5$ (exposure category B)

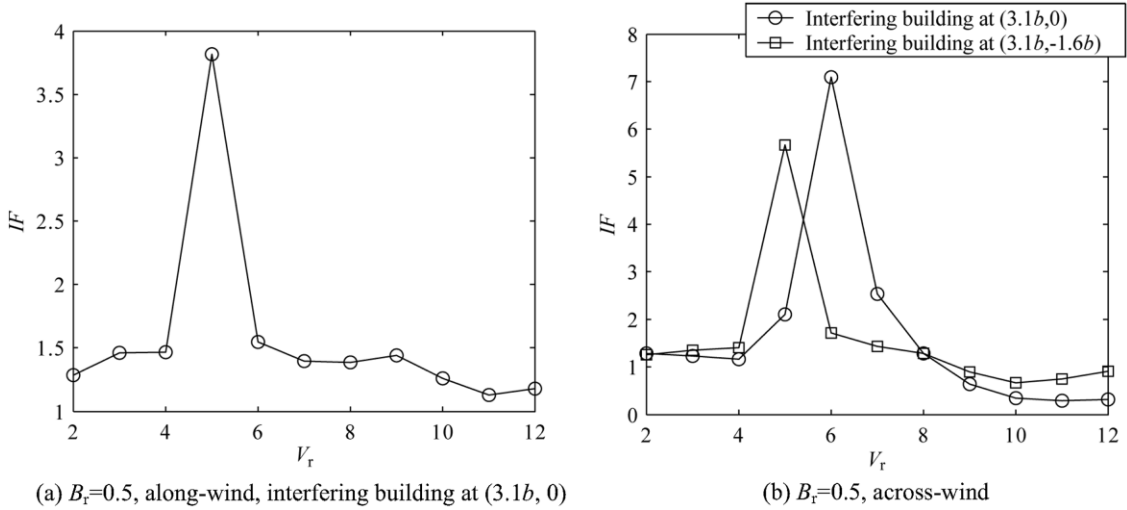


Fig. 8 Variations of the dynamic interference factors with the reduced velocity (exposure category B)

dominant frequencies in the approach flow caused by the vortex shedding from the interfering building of $B_r=0.5$ are centered at a reduced frequency of about 0.17~0.2. And finally, this leads to the resonance occurring at lower reduced velocity ranges of $V_r=5\sim 6$.

3.3.2. Effect of height ratio

3.3.2.1. Mean interference effect

The mean interference factor $RIF(x/b, y/b)$ of the four configurations of $H_r=0.5, 0.75, 1.25$ and 1.5 have pronounced correlations with that of the configuration of $H_r=1$, with the correlation

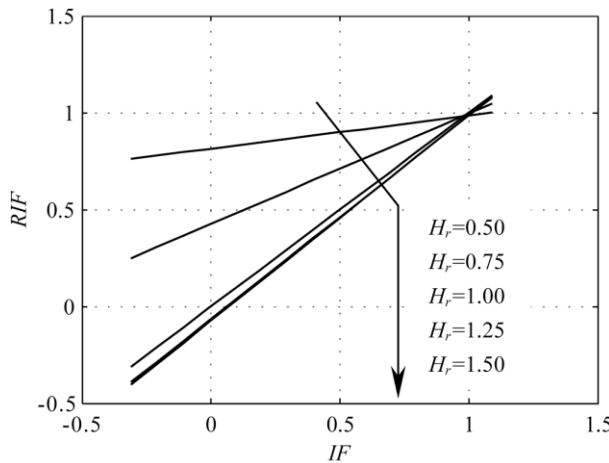


Fig. 9 Regression results of the mean *IF* for the configuration of different height ratios (in exposure category B)

coefficient ρ ranging from 0.93 to 0.99 and the maximum residual ε of only 0.05. The regression curves of the mean *RIF* for the configurations of different height ratios are shown in Fig. 9, which indicates that the shielding effects of the interfering building decrease with the decrease of H_r and become negligible when $H_r < 0.5$. The interference factors decrease rapidly, that is to say, the shielding increases rapidly, with the increase of H_r in the range between 0.5 and 1.0.

In contrasting to the significant difference of the *IFs* of the interfering buildings with $H_r = 0.5$, 0.75 and 1.0, the interference factors vary slightly for the interfering buildings of $H_r \geq 1$, and the two regression curves of $H_r \geq 1.25$ are almost the same (see Fig. 9). This means the shielding keeps unchanged when $H_r \geq 1.25$.

According to the above discussion, the mean *IF* of the different height ratios can be simply predicted from the results of the two identical buildings as shown in Fig. 3(a) by

$$RIF = \begin{cases} 1 & (H_r < 0.5) \\ 0.815 + 0.171IF & (H_r = 0.5) \\ 0.426 + 0.569IF & (H_r = 0.75) \\ IF & (H_r = 1.0) \\ -0.073 + 1.062IF & (H_r \geq 1.25) \end{cases} \quad (10)$$

3.3.2.2. Dynamic interference effect

Considering the effects of the height ratio on the dynamic interference factors, the distributions of the *EIfs* between different height ratios still show good linear correlations. Fig. 10 presents the regression results of the across-wind *EIf* for different height ratios.

From Fig. 10 it can be seen that the dynamic interference effects increase with the height of the interfering building whilst the effects of the interfering building of $H_r < 0.5$ can be neglected. Generally, the regression results of the along-wind *EIfs* of the configurations of different height ratios show the similar tendency with those of the across-wind direction. Therefore, the variations of

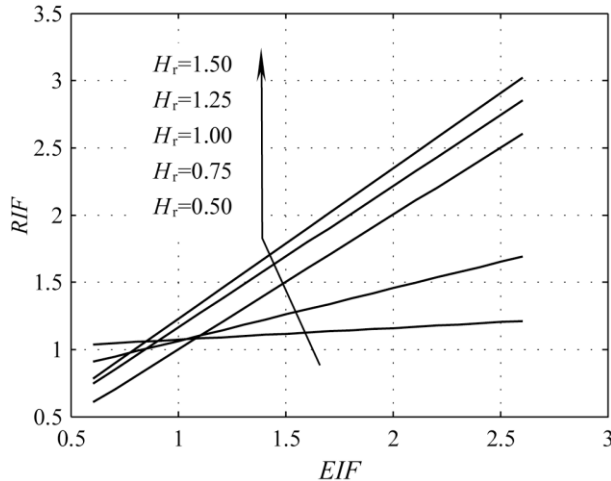


Fig. 10 Regression results of the across-wind envelope interference factors for the configuration of different height ratios (exposure category B)

Table 3 Regression coefficients of the envelope interference factors for the configurations of different height ratios

H_r	Along-wind		Across-wind	
	C_0	C_1	C_0	C_1
0.50	1.060	0.043	0.986	0.087
0.75	0.808	0.339	0.670	0.392
1.25	0.466	0.850	0.108	1.053
1.50	0.089	1.197	0.107	1.119

the EIF with the height ratios in the two directions can be expressed by

$$RIF = C_0 + C_1 IF \quad (11)$$

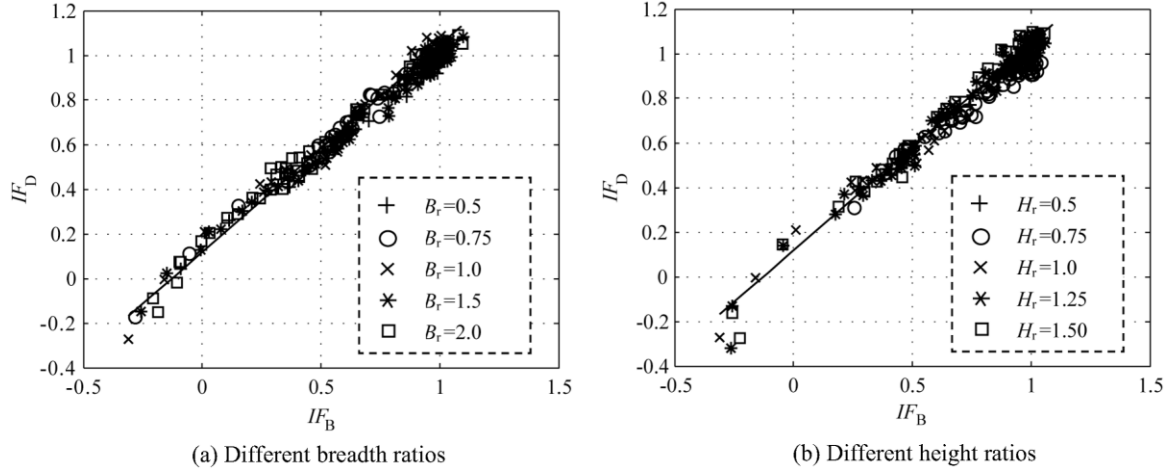
where C_0 and C_1 are the regression coefficients and vary with the height ratio and direction listed in Table 3.

Different from the above discussed mean interference factors, the regression results show that the dynamic interference factors for $H_r = 1.5$ still have an increase of 20% and 12% over those of $H_r = 1.25$ in the two directions respectively. The results also show that the dynamic interference factors still increase rapidly with the increase of H_r from 0.5 to 1.0.

3.3. Effects of upstream terrains

3.3.1. Mean interference effect

Fig. 11 presents the variations of the mean IF for the configurations of different height ratios and breadth ratios in the exposure categories D with those in category B.

Fig. 11 Correlations of the mean *IFs* between different upwind terrains

In Fig. 11, IF_B and IF_D are the mean *IF* in exposure categories B and D respectively. It can be seen from the figures that the significant linear correlations exist in the distributions of the interference factors between the two upwind terrains for all the discussed configurations. With the regression, the mean *IF* of any configuration in exposure category D can be easily predicated from the corresponding mean *IF* in exposure category B by

$$IF_D = 0.119 + 0.928IF_B \quad (12)$$

3.3.2. Dynamic interference effect

For dynamic interference effects, the degree of the correlation of the *EIfs* between exposure categories B and D is not so strong as that of the mean *IF* discussed above. Fig. 12 shows the

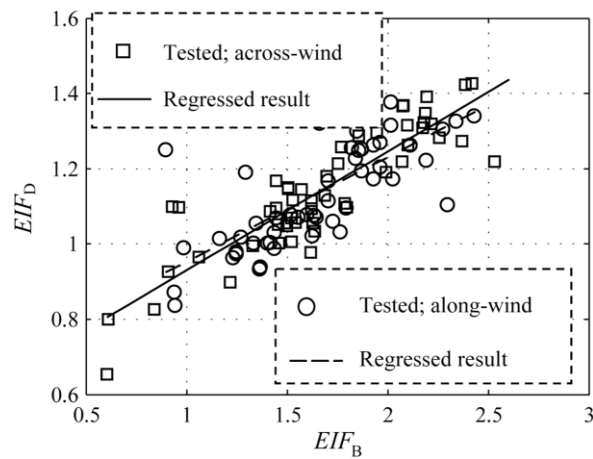


Fig. 12 Correlations of the envelope interference factors between exposure categories B and D

Table 4 Regression coefficients of the envelope interference factors between exposure categories B and D

B_r	H_r	Along-wind		Across-wind	
		C_0	C_1	C_0	C_1
0.5	1.0	0.823	0.189	0.792	0.210
0.75	1.0	0.814	0.206	0.769	0.174
1.0	1.0	0.675	0.287	0.614	0.316
1.5	1.0	0.896	0.278	0.531	0.333
2.0	1.0	0.896	0.180	0.601	0.329
1.0	0.50	0.764	0.279	1.026	0.093
1.0	0.75	0.697	0.220	0.636	0.291
1.0	1.25	0.735	0.248	0.546	0.311
1.0	1.5	0.913	0.214	0.807	0.318

comparison of the *EIFs* of the configuration of two identical buildings between exposure categories B and D. It can be found that the data still show a good correlation with the correlation coefficients ρ of 0.80 and 0.88 in the along-wind direction and the across-wind direction, respectively; and the maximum residual ε of only 0.09.

In Fig. 12, EIF_B and EIF_D are the *EIF* in exposure categories B and D respectively. Similar to the configuration of two identical buildings, linear correlations still exist in the *EIFs* of the other configurations between the two upstream terrains. Generally, the relation of the *EIFs* between the two upstream terrains for all the discussed configurations can be expressed by

$$EIF_D = C_0 + C_1 EIF_B \quad (13)$$

where C_0 and C_1 are the regression coefficients, which vary with the height ratio and direction, and are listed in Table 4.

4. Conclusions

Many factors can affect the wind loads on a building under interference excitations from another interfering building. The effects of upstream terrain conditions, reduced velocity, relative heights and breadths of the interfering building, and the spacing between these two buildings have been investigated in a series of deliberate wind tunnel tests. Some of the main results are summarized below:

- (1) For mean interference effects, an upstream building usually provides shielding effects to a principal building and the corresponding interference factors are generally less than 1.0. Larger upstream buildings could produce more serious shielding effects on the principal building. While the shielding effects become negligible when the height ratio of the buildings $H_r < 0.5$ and keep unchanged when $H_r \geq 1.25$. Linear regression formulas are derived to describe the relations between the mean *IF* values for different height ratios and breadth ratios.
- (2) The breadth ratio can significantly affects the dynamic interference effects. Special attention should be paid to the interference effects from a smaller breadth upstream interfering building, since this type of building can induce the resonance on the downstream building at a lower

reduced velocity and produce higher interference factors which are usually several times greater than the non-resonance case. A higher interfering building produces stronger dynamic interference effects on the principal building whilst the effect of the interfering building with $H_r < 0.5$ can be neglected. The regression analyses indicate linear correlations between the dynamic interference factors for different height ratios, and the corresponding formulas are given.

- (3) The effects of the upwind terrain conditions are quantitatively analyzed by correlation and regression analyses, and the results show that significant correlations exist in the distributions of the interference factors, especially the mean interference factors, of different upwind terrains and. And thus some relevant regression formulas are proposed to simplify the complexity of the wind induced interference effects between two tall buildings.

Acknowledgements

This research is jointly supported by the National Science Foundation (50478118, 50321003), the Foundation for University Key Teachers by the Ministry of Education, and the Science Foundation of Guangdong Province (010455). Their supports are gratefully acknowledged.

References

- Bailey, P.A. and Kwok, K.C.S. (1985), "Interference excitation of twin tall buildings", *J. Wind Eng. Ind. Aerodyn.*, **21**, 323-338.
- English, E.C. (1993), "Shielding factors for paired rectangular prism: an analysis of along-wind mean response data from several source", *Proc. 7th US National Conf. Wind Engineering, University of California, Los Angeles, CA, USA*.
- English, E.C. and Fricke, F.R. (1999), "The interference index and its prediction using a neural network analysis of wind-tunnel data", *J. Wind Eng. Ind. Aerodyn.*, **83**, 567-575.
- GB50009-2001 (2002), Chinese Load code for design of building structures.
- Khanduri, A.C., Bedard, C. and Stathopoulos, T. (1997), "Modelling wind-induced interference effects using backpropagation neural networks", *J. Wind Eng. Ind. Aerodyn.*, **72**, 71-79.
- Khanduri, A.C., Stathopoulos, T. and Bédard, C. (1998), "Wind-induced interference effects on buildings - a review of the state-of-the-art", *Eng. Struct.*, **20**(7), 617-630.
- Sakamoto, H. and Hanju, H. (1988), "Aerodynamic forces acting on two square prisms placed vertically in a turbulent boundary layer", *J. Wind Eng. Ind. Aerodyn.*, **31**, 41-66.
- Taniike, Y. and Inaoka, H. (1988), "Aeroelastic behaviour of a tall building in wakes", *J. Wind Eng. Ind. Aerodyn.*, **28**, 317-327.
- Taniike, Y. (1991), "Turbulence effect on mutual interference of buildings", *J. Eng. Mech., ASCE*, **117**(3), 443-456.
- Taniike, Y. (1992), "Interference mechanism for enhanced wind forces on neighbouring tall buildings", *J. Wind Eng. Ind. Aerodyn.*, **41**, 1073-1083.
- Tschanz, T. and Davenport, A.G. (1983), "The base balance technique for the determination of dynamic wind loads", *J. Wind Eng. Ind. Aerodyn.*, **13**, 429-439.
- Zhang, W.J., Kwok, K.C.S. and Xu, Y.L. (1994), "Aeroelastic torsional behaviour of tall buildings in wakes", *J. Wind Eng. Ind. Aerodyn.*, **51**, 229-249.